Available online at www.sciencedirect.com
SCIENCE DIRECT®
Journal of Nuclear Materials 329–333 (2004) 1451–1455
journal of nuclear materials
www.elsevier.com/locate/jnucmat

Influence of an electric field on the microstructure evolution of ion-irradiated alumina

K. Yasuda *, K. Tanaka, M. Shimada, T. Yamamoto, S. Matsumura, C. Kinoshita

Department of Applied Quantum Physics and Nuclear Engineering, Kyushu University, Hakozaki 6-10-1, Fukuoka 812-8581, Japan

Abstract

Radiation-induced defects in α-alumina were investigated through transmission electron microscopy for specimens irradiated with 100 keV He^+ ions at 760 K with an electric field of 100 kV/m. Ion-irradiation with an electric field induces characteristic defect clusters, such as bundles of long-shaped defect clusters, aluminum colloid and γ-alumina precipitates, and interstitial type-dislocation loops, though only dislocation loops were formed when the material is irradiated without an electric field. Electron microscopy analysis has revealed the lattice displacement vector of long-shaped defects, and the crystallographic relationship among α-alumina matrix, aluminum colloid and γ-alumina.

1. Introduction

α-Alumina, α-Al_2O_3, has potential applications for insulators and rf-windows in ITER, and will be subjected to simultaneous displacement damage and electronic excitation with an applied electric field from 10 to 10^4 kV/m [1]. The most crucial problem for insulators under such radiation environments is radiation induced electrical degradation (RIED), which manifests itself as a permanent increase in electrical conductivity. This catastrophic degradation of insulating ability was originally found by Hodgson in polycrystalline α-Al_2O_3 [2]. They showed that an electric field of 180 kV/m stabilizes F^- centers induced by 1.8 MeV electron irradiation, and proposed that an electric field enhances oxygen vacancy aggregation and induces γ-Al_2O_3 formation [3,4].

It has been shown that point defects in ionic crystals carry an electric charge, and their migration and recombination processes are controlled by the Coulomb force of surrounding charges [5,6]. The nucleation-and-growth processes of radiation-induced defects are, therefore, considered to be influenced by an applied electric field. The present authors have investigated the formation process of interstitial-type dislocation loops in ion-irradiated α-Al_2O_3 at 760 K under an electric field of 100 kV/m, and revealed that the electric field suppresses the nucleation of interstitial-type dislocation loops and enhances their growth [7,8]. A higher fraction of interstitials has been found to annihilate at surface sinks in thin-foil specimens due to a significant contribution of directional migration of interstitials driven by the electric field [8].

In the present paper, we report radiation-induced defects in α-Al_2O_3 formed under irradiation with 100 keV He^+ ions in the presence of an applied electric field. Special attention is placed on analysis of anomalous defect clusters and precipitates of aluminum colloids and/or γ-Al_2O_3, which were characteristically formed in specimens irradiated with an electric field of 100 kV/m.

2. Experimental

Single crystals of α-Al_2O_3 (supplied by Bicron Ltd.), whose surfaces were oriented parallel to $(1\,1\,\bar{2}\,0)$ planes, were used in the present study. Electron-transparent specimens for TEM were prepared from disk-shaped

* Corresponding author. Tel.: +81-92 642 3773; fax: +81-92 642 3771.
E-mail address: yasudak@nucl.kyushu-u.ac.jp (K. Yasuda).

0022-3115/$ - see front matter © 2004 Elsevier B.V. All rights reserved.
doi:10.1016/j.jnucmat.2004.04.160

specimens with 3 mm diameter and 100 μm thickness by dimpling and ion-thinning with 4 keV Ar^+ ions to make a small hole at the center. The thin-foil specimens were annealed in air at 1470 K for 2 h to eliminate defects induced during Ar^+-ion thinning. Thin titanium layers (<0.1 μm in thickness) were deposited in vacuum as electrodes on both surfaces of the specimen with a width of 0.5 mm. The distance between electrodes was 2 mm. The specimen was mounted in a sample holder specially developed by the present authors, which enabled irradiation in an ion-accelerator at high temperatures in the presence of an electric field. The details of the specimen holder, and the specimen and electrode configurations are described elsewhere [9].

The thin-foil specimens were irradiated with 100 keV He^+ ions at 760 K with an applied DC voltage of 200 V up to a fluence of 1.3×10^{20} ions/m^2. The electric field is applied parallel to the specimen surface with a nominal value of $E = 100$ kV/m. The actual value of E in the observed region of the wedge-shaped thin-foil specimen is, however, expected to be complicated. A finite element simulation code of ANSYS [9] was applied to a model crystal possessing the same configuration as the specimen used in the present study. The values of E were dependent on the local position in the thin foil specimen, and the maximum value was observed at a position parallel to the electrodes was predicted to be about three times larger than the nominal value of E. Displacement damage was evaluated to be about 0.5 dpa by using SRIM-2000, with displacement energies of 20 eV for Al ions and 50 eV for O ions [10]. About ~98% incident ions were found to pass through the thin-foil specimens at thicknesses less than ~200 nm, where TEM observations were performed. Microstructures of these irradiated specimens were analyzed with the weak-beam dark-field (WBDF) technique and selected area electron diffraction (SAED) with a JEM-2000EX operated at 200 kV.

3. Results and discussion

Fig. 1 shows the microstructure of α-Al_2O_3 irradiated at 760 K with 100 keV He^+ ions with an applied electric field of 100 kV/m, indicating the presence of dislocation loops as tiny dot-contrast features (indicated as A), and long-shaped defect clusters (indicated as B). It should be emphasized here that the defect clusters B were observed only in the specimen irradiated with an electric field. The defects B were observed heterogeneously in the specimen with developing bundles as shown in Fig. 1, and were seen to elongate in a [0 0 0 1] direction, irrespective of the direction of the electric field. No systematic correlation was been found between the location where defect B is formed and the position of the electrode. In contrast, dislocation loops were formed homogeneously in both

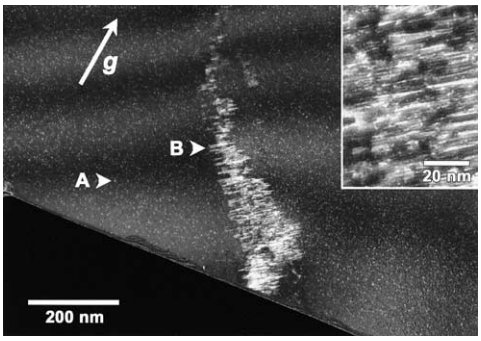

Fig. 1. Typical example of WBDF images of a α-alumina irradiated with 100 keV He^+ ions at 760 K with $E = 100$ kV/m. Tiny dot-contrast features of interstitial-type dislocation loops (indicated as A) and anomalous defect clusters (indicated as B) were seen. The upper right-hand photograph is the magnified microstructure of defect B. The electron-bean incident direction is $B = \langle 1\,1\,\bar{2}\,0\rangle$, and utilized diffraction condition is $g = 1\,0\,\bar{1}\,2$ ($2g$–$6g$).

specimens irradiated with and without the electric field. However, the electric field of 100 and 300 kV/m has significantly influenced the nucleation-and-growth process of dislocation loops, that is, an electric field suppresses the nucleation of dislocation loops but enhances their growth [7,8].

Fig. 2 illustrates the defect B taken with different reflections. The $g \cdot R_n$ analysis, where g and R_n are the diffraction vector and the lattice displacement vector respectively, reveals that the diffraction contrast of the defects B disappears with $g = 0\,0\,0\,6$ and $g = \bar{2}\,1\,1\,0$. This demonstrates that the defect B possesses a lattice displacement vector parallel to $\langle 0\,1\,\bar{1}\,0\rangle$, and suggests that the defect B is a planar defect, such as a dislocation loop or stacking fault.

A selected area electron diffraction (SAED) pattern from the regions where bundles of defects B are formed is shown in Fig. 3. Parts of Debye rings are seen in the SAED pattern in addition to diffraction spots of α-Al_2O_3 matrix. Table 1 summarize the interplanar spacing, d_{hkl}, evaluated for the Debye rings shown in Fig. 3 by using the relationship, $r_{hkl} \cdot d_{hkl} = \lambda \cdot L$, where λ is the wavelength of 200 keV electrons (0.0251 Å), L camera length (1200 mm) and r_{hkl} is the distance between the direct beam and individual Debye rings on a film. The evaluated values of d_{hkl} show good agreements with those of Al metal and part of γ-Al_2O_3. However, it is arduous to distinguish Al and γ-Al_2O_3 solely from the values of d_{hkl} shown in Fig. 3 since the lattice constant of Al metal (4.05 nm) is nearly one half of that of γ-Al_2O_3 (8.0 nm [11]), and both crystals belong to fee-base cubic structure.

To proceed further with the analysis, SAED patterns were taken from different incident electron-beam directions. Fig. 4(a) presents an SAED pattern for the [1 $\bar{2}$ 1 0]

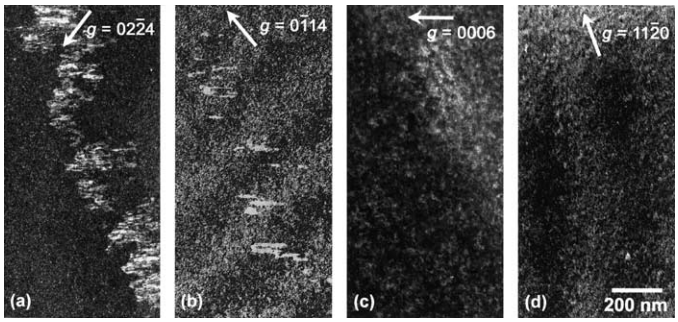

Fig. 2. Long-shaped defect clusters (defect B) taken with different refractions for $g = 10\bar{1}\bar{2}$ (a), $g = \bar{1}01\bar{4}$ (b), $g = 000\bar{6}$ (c) and $g = \bar{2}110$ (c). (c) and (d) are taken from the identical region with (a), and (b) is from the vicinity of (a).

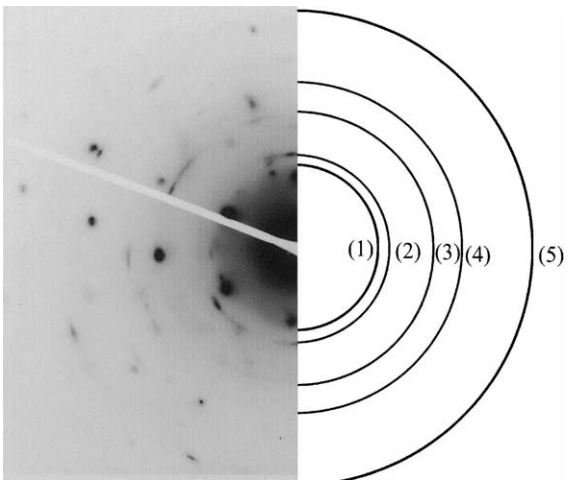

Fig. 3. A SAED pattern of α-Al_2O_3 including bundles of long-shaped defect clusters, irradiated with 100 keV He^+ ions with an electric field of 100 kV/m. The incident electron beam direction is close to $[0\bar{4}41]$ of α-Al_2O_3 matrix.

Table 1
Experimentally measured interplanar spacing (d^{exp}) and calculated ones of Al metal (d^{Al}) and γ-alumina ($d^{\gamma\text{-}Al_2O_3}$)

Experiment, d^{exp} (Å)	Al metal, d^{Al}	γ-Al_20_3, $d^{\gamma\text{-alumina}}$	$\lvert F_{hkl}\rvert^2/F_{400}\rvert^2$
		$d_{111} = 4.62$	0.055
		$d_{220} = 2.83$	0.118
		$d_{311} = 2.42$	0.323
(1) 2.30	$d_{111} = 2.34$	$d_{222} = 2.31$	0.023
(2) 2.01	$d_{200} = 2.02$	$d_{400} = 2.00$	1.000
(3) 1.40	$d_{220} = 1.43$	$d_{440} = 1.41$	1.439
(4) 1.20	$d_{311} = 1.22$	$d_{444} = 1.15$	0.415
(5) 1.01	$d_{400} = 1.01$	$d_{800} = 1.00$	0.431

Values of $|F_{hkl}|^2/|F_{400}|^2$ are also shown for γ-Al_2O_3, which were calculated with an assumption of random occupation of Al ions on octahedral and tetrahedral sites.

zone axis, which clearly shows extra spots in addition to those of α-Al_2O_3. These extra spots are indexed as belonging to the $[\bar{1}12]$ zone axis of γ-Al_2O_3 and the [1 1 1] zone axis of Al metal (Fig. 4(c)). Apart of Debye rings are also seen at the lattice space of the 2 2 0 Al reflection. Similarly, the extra spots appearing on a SAED pattern for the $[2\bar{4}23]$ zone axis were indexed as belonging to the $[\bar{1}10]$ zone axis of γ-Al_2O_3 and the [0 1 0] zone axis of Al metal (Fig. 4(b) and (d)). Since the angles between the zone axes shown in Fig. 4(a) and (b), that is $[1\bar{2}10]$ and $[2\bar{4}23]$ for α-Al_2O_3, $[\bar{1}12]$ and $[\bar{1}10]$ for γ-Al_2O_3, and [1 1 1] and analysis [0 1 0] for Al metal, are almost identical, the results indicate that most of precipitates are not oriented randomly but possess a preferential crystallographic relationship as

$$\alpha\text{-}Al_2O_3\langle 1\bar{2}10\rangle//Al\langle 111\rangle//\gamma\text{-}Al_2O_3\langle\bar{1}12\rangle.$$

Furthermore, from the coincidence of diffraction spots in Fig. 4 (labeled with a large open circle in Fig. 4(c) and (d)), one can obtain a preferential relationship regarding habit planes among precipitates and matrix as

$$\alpha\text{-}Al_2O_3(10\bar{1}0)//Al(\bar{1}01)//\gamma\text{-}Al_2O_3(110).$$

Fig. 5 compares a WBDF image taken from a $(20\bar{2}4)$ reflection of the α-Al_2O_3 matrix (a) and a centered dark-field image taken from an extra diffraction spot (b) indexed as Al metal in identical regions. Defects exhibiting white dot contrast, whose size is about 10–20 nm, are seen uniformly in Fig. 4(b), whereas long-shaped defects and dislocation loops are seen in (a). The contrast shown in (b) is entirely different from that of dislocation loops [7,12,13]. Precipitates of γ-Al_2O_3 are also confirmed through WBDF images.

As described above, our TEM analyses clearly show that an electric field induces characteristic defects in α-Al_2O_3, such as long-shaped defects, and the precipitation of Al colloids and γ-Al_2O_3, in addition to dislocation loops. This implies that charge neutrality is not retained in specimens irradiated in the presence of an electric field, and the nucleation of nonstoichiometric

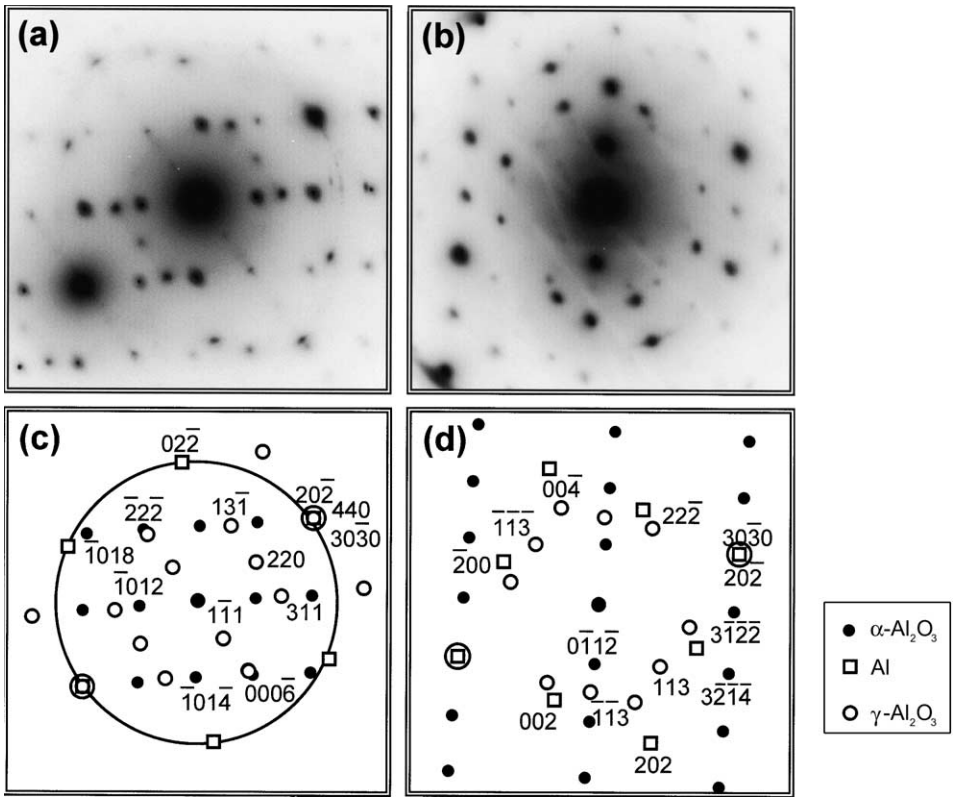

Fig. 4. SAED patterns of α-Al_2O_3 taken with imaging plates for the zone axes of $[1\,\bar{2}\,1\,0]$ (a) and $[2\,\bar{4}\,2\,3]$ (b). (c) and (d) are the indexed patters as belonging Al $[1\,1\,1]$ zone axis and γ-Al_2O_3 $[\bar{1}\,1\,2]$ zone axis (c) and Al $[0\,1\,0]$ zone axis and γ-Al_2O_3 $[\bar{1}\,1\,0]$ zone axis. Extra spots superimposed with three phases are labelled with large open circles in (c) and (d).

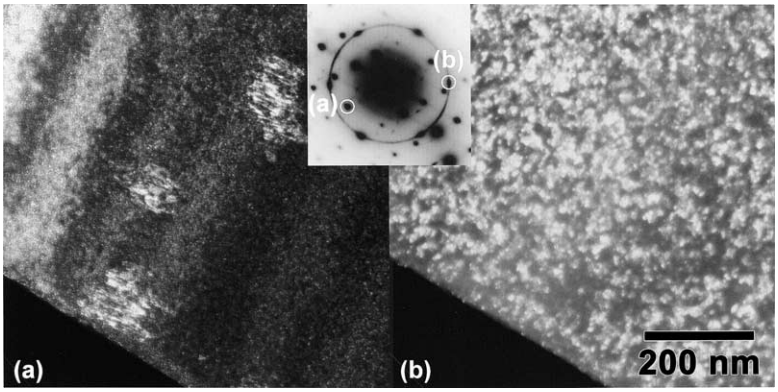

Fig. 5. A comparison of microstructure showing bundles of long-shape defect clusters and Al colloids in the identical region taken from different diffraction spots of (a) and (b), respectively. The electron-bean incident direction is $B = \langle 1\,1\,\bar{2}\,0\rangle$.

defect clusters is stabilized. Pells and Hodgson [4] observed very large precipitates of γ-Al_2O_3 ($\sim$0.1–2 μm in size) in α-Al_2O_3, irradiated with 1.8 MeV electrons at 730 K with an electric field of 130 kV/m, and discussed that an electric field stabilizes may F^+ centers [3] to promote aggregation of F_2 centers (or oxygen vacancy clusters), leading to a phase transformation to an Al-rich phase of γ-Al_2O_3.

Kinoshita et al. [14] have shown that dislocation loops change their Burgers vector as $\frac{1}{3}[0\,0\,0\,1] \rightarrow$

$\frac{1}{3}\langle 1\,0\,\bar{1}\,0\rangle \rightarrow \frac{1}{3}\langle 1\,0\,\bar{1}\,1\rangle$ to be converted from faulted loops to unfaulted ones, with increasing size. Therefore, a speculation for the formation of long-shaped defects is that faulted loops with $b = \frac{1}{3}\langle 1\,0\,\bar{1}\,0\rangle$ are stabilized to grow in a particular $\langle 0\,0\,0\,1\rangle$ direction, due to the directed migration of interstitials under the an influence of the electric field. This may change the defect kinetics to promote precipitation of Al colloids and γ-Al_2O_3, although further work is necessary to provide an understandings the physical mechanisms. It is also interesting to note that the size of Al collides (10–20 nm) is larger than that of γ-Al_2O_3. This is possibly explained by the phase transformation from γ-Al_2O_3 to Al colloids with increasing size or irradiation fluence. This may explain why only the γ-Al_2O_3 phase was observed in α-Al_2O_3 [5] reported by Pells et al., which were subjected to a low level of displacement damage ($\sim 10^{-5}$ dpa) with 1.8 MeV electrons under an electric field of 130 kV/m.

4. Conclusions

We have investigated through transmission electron microscopy the nucleation-and-growth process of defect clusters in α-Al_2O_3 irradiated with 100 keV He^+ ions with an applied electric field of 100 kV/m. The main conclusions are drawn as follows.

(1) Irradiation with an electric field induces long-shaped defect clusters which are elongated in the [0 0 0 1] direction having a lattice displacement vector of $\langle 1\,\bar{1}\,0\,0\rangle$, precipitation of Al colloids and γ-Al_2O_3, and interstitial-type dislocation loops.
(2) Al colloids and γ-Al_2O_3 precipitates were formed heterogeneously in specimens, and are observed solely at regions where long-shaped defects were observed.
(3) SAED pattern analysis revealed the following crystallographic relationship among the three phases: α-$Al_2O_3\langle 1\bar{2}10\rangle // Al\langle 111\rangle // \gamma$-$Al_2O_3\langle \bar{1}12\rangle$, α-Al_2O_3-$(10\bar{1}0) // Al(\bar{1}01) // \gamma$-$Al_2O_3(110)$. A part of precipitates were formed with a random orientation constituting parts of Debye rings in SAED patterns.
(4) An electric field is found to change not only the density and size of defect clusters but also the morphology and nature of defect clusters, which are considered to influence the physical properties of insulating ceramics, such as RIED phenomenon.

Acknowledgements

A part of TEM experiments were carried out at the HVEM laboratory, Kyushu University. We are grateful to M. Kutsuwada of Kyushu University for his assistance to ion irradiations. This work was supported in part by TEPCO research foundation and Japan Nuclear Cycle Development Institute (JNC).

References

[1] T. Shikama, K. Yasuda, S. Yamamoto, C. Kinoshita, S.J. Zinkle, E.R. Hodgson, J. Nucl. Mater. 271&272 (1999) 560.
[2] E.R. Hodgson, Cryst. Latt. Def. Amorph. Mater. 18 (1989) 169.
[3] E.R. Hodgson, A. Moroño, J. Nucl. Mater. 283 (2000) 880.
[4] G.P. Pells, E.R. Hodgson, J. Nucl. Mater. 226 (1995) 291.
[5] C. Kinoshita, Y. Isobe, H. Abe, Y. Denda, T. Sonoda, J. Nucl. Mater. 206 (1993) 341.
[6] E.A. Kotomin, A.I. Popov, Nucl. Instrum. and Meth. B 141 (1998) 1.
[7] K. Yasuda, T. Higuchi, K. Shiiyama, C. Kinoshita, K. Tanaka, M. Kutsuwada, Phil. Mag. Lett. 83 (2003) 21.
[8] T. Higuchi, K. Yasuda, K. Shiiyama, M. Kutsuwada, C. Kinoshita, Nucl. Instrum. and Meth. B 206 (2003) 103.
[9] http://www.ansys.com.
[10] S.J. Zinkle, C. Kinoshita, J. Nucl. Mater. 251 (1997) 200.
[11] H. Konig, Naturwissenschafen 35 (1948) 92.
[12] K. Yasuda, C. Kinoshita, Nucl. Instrum. and Meth. B 191 (2002) 559.
[13] K. Yasuda, C. Kinoshita, M. Ohmura, H. Abe, Nucl .Instrum. and Meth. B. 166&167 (2000) 107.
[14] C. Kinoshita, S. Matsumura, K. Yasuda, T. Soeda, M. Noujima, Mat. Res. Soc. Symp. Proc. 540 (1999) 287.